7-2004

Effect of Ventilation Rate on Instilled Surfactant Distribution in the Pulmonary Airways of Rats

Joseph C. Anderson
Marquette University

Robert C. Molthen
Marquette University, robert.molthen@marquette.edu

Christopher A. Dawson
Medical College of Wisconsin

Steven Thomas Haworth
Marquette University

Joseph L. Bull
University of Michigan - Ann Arbor

See next page for additional authors

Journal of Applied Physiology, Vol. 97, No. 1 (July 2004): 45-56. DOI.

Effect of Ventilation Rate on Instilled Surfactant Distribution in The Pulmonary Airways of Rats

Joseph C. Anderson
Department of Biomedical Engineering, University of Michigan, Ann Arbor, Michigan
Robert C. Molthen
Marquette University and Medical College of Wisconsin, Milwaukee, Milwaukee, Wisconsin
Zablocki Veterans Affairs Medical Center, Milwaukee, Wisconsin
Christopher A. Dawson
Marquette University and Medical College of Wisconsin, Milwaukee, Milwaukee, Wisconsin
Zablocki Veterans Affairs Medical Center, Milwaukee, Wisconsin
Steve T. Haworth
Marquette University and Medical College of Wisconsin, Milwaukee, Milwaukee, Wisconsin
Zablocki Veterans Affairs Medical Center, Milwaukee, Wisconsin

Joseph L. Bull
Department of Biomedical Engineering, University of Michigan, Ann Arbor, Michigan
Matthew R. Glucksberg
Department of Biomedical Engineering, Northwestern University, Evanston, Illinois
James B. Grotberg
Department of Biomedical Engineering, University of Michigan, Ann Arbor, Michigan

Abstract

Liquid can be instilled into the pulmonary airways during medical procedures such as surfactant replacement therapy, partial liquid ventilation, and pulmonary drug delivery. For all cases, understanding the dynamics of liquid distribution in the lung will increase the efficacy of treatment. A recently developed imaging technique for the study of real-time liquid transport dynamics in the pulmonary airways was used to investigate the effect of respiratory rate on the distribution of an instilled liquid, surfactant, in a rat lung. Twelve excised rat lungs were suspended vertically, and a single bolus (0.05 ml) of exogenous surfactant (Survanta, Ross Laboratories, Columbus, OH) mixed with radiopaque tracer was instilled as a plug into the trachea. The lungs were ventilated with a 4-ml tidal volume for 20 breaths at one of two respiratory rates: 20 or 60 breaths/min. The motion of radiodense surfactant was imaged at 30 frames/s with a microfocal X-ray source and an image intensifier. Dynamics of surfactant distribution were quantified for each image by use of distribution statistics and a homogeneity index. We found that the liquid distribution depended on the time to liquid plug rupture, which depends on ventilation rate. At 20 breaths/min, liquid was localized in the gravity-dependent region of the lung. At 60 breaths/min, the liquid coated the airways, providing a more vertically uniform liquid distribution.

Keywords

surfactant replacement therapy; respiratory distress syndrome; drug delivery; exogenous lung surfactant; liquid bolus instillation

Direct instillation of a liquid bolus into the lung occurs during surfactant replacement therapy, which is now a standard treatment for neonates with respiratory distress syndrome (5, 18, 19, 24). In some studies, it has reduced infant mortality by half (24). The instilled bolus has been studied either as a prophylactic dose at birth or as rescue doses given several hours after delivery (19). The intratracheal bolus spreads by a combination of various physical forces. The initial spreading can be quite rapid (2, 6), reaching substantial portions of the lung fields in 20 s. The early response of improved oxygenation for the patient appears to result from an increase in functional residual capacity (4, 13) when increased tidal volumes are used rather than end-expiratory volume (20).

Exogenous surfactant administration also has been used with varying degrees of success as a therapy for acute respiratory distress syndrome (23, 33), for mitigation of oxygen-toxic lung injury (25, 29) and wood smoke inhalation injury (10), for improvement of lung transplant results (26), for treatment of ventilation-induced lung injury (38), and for treatment of meconium aspiration (27, 42). It has been effective in animal models of saline-lavage lung injury for pigs (34) and sheep (22). Another instance of liquid instillation into the lung occurs with perfluorocarbons used for partial liquid ventilation (11, 21, 36, 43) or used as a vehicle for delivery of medications such as antibiotics (7, 32) or genetic material (40, 41).

In surfactant replacement therapy, several parameters involving the physiology and the applied technique may affect surfactant transport (31): the bolus volume (12), its injection rate (9, 37), gravity and orientation (37), development of airway occlusion by the liquid (2, 8), ventilation parameters at normal or high frequency (16, 30), alveolar recruitment (4, 13, 20), the viscosity and surface tension of the fluid instilled, the dose strength, the instillation site, and repeat dosing protocols and intervals.

In Cassidy et al. (2), our laboratory showed that the method of liquid instillation affects how the liquid distributes within the lung. In that study, exogenous surfactant (Survanta) mixed with a radiopaque tracer was instilled into tracheae of vertical, excised rat lungs (ventilation 40 breaths/min, 4 ml tidal volume). Two methods of liquid instillation were examined and compared: *1*) liquid drains by gravity into the upper airways followed by inspiration; and *2*) the liquid initially forms a plug in the trachea, followed by inspiration. The experiments were imaged via X-rays and were continuously recorded at 30 frames/s. The fluid transport dynamics of the initial breaths were quantified statistically and were shown to follow trends for liquid plug propagation theories. We found that the formation of a liquid plug in the trachea before the first inspiration results in a liquid distribution that is twice as homogeneous as instillation by gravity-driven liquid draining. From that study, we concluded that the formation of a liquid plug in the trachea, before inspiration, is important in creating a more uniform liquid distribution throughout the lungs.

Research on liquid plug or bubble propagation in conduits spans a number of applications ranging from oil recovery in porous rock to liquid instillation in the lung. Theories have been developed for rigid tubes (1, 39), rigid channels (14), flexible tubes (17), and branching tube networks such as the lung (8, 15). One of the key results is that when a liquid plug with viscosity μ, density ρ, and constant surface tension σ propagates at speed U inside a tube of radius a, it deposits a trailing film along the tube wall whose thickness, h, depends on these parameters. In the simplest case, in which viscous forces are large and gravitational and inertial forces are negligible, the thickness of the trailing film h can be determined as a function of the propagation speed U and the other parameters in a dimensionless relation of the form $h/a = \phi(\mathrm{Ca})$ where $\mathrm{Ca} = \mu U/\sigma$ is the capillary number. In general, the trailing film thickness increases as Ca increases. For $\mathrm{Ca} \ll 1$, $\phi(\mathrm{Ca}) \approx \mathrm{Ca}^{2/3}$ (1, 28), whereas for arbitrary Ca the numerical results in Ref. 15 are well fit by the curve $\phi(\mathrm{Ca}) = 0.36[1-\exp(-2\mathrm{Ca}^{0.523})]$. This latter expression asymptotes to $\phi(\mathrm{Ca}) = 0.36$ as $\mathrm{Ca} \rightarrow \infty$, which correlates to the experimental results in Ref. 35.

In the present study, we investigate the effect of breathing frequency on the distribution of an instilled liquid plug in excised rat lungs. The purpose is to understand better the interplay of plug propagation dynamics discussed above with gravitational mechanisms of transport. Because the trailing film thickness decreases with smaller plug speeds, benchtop experiments (3) have shown that a liquid plug traveling at a slow speed in a tube remains intact for a longer period of time until it ruptures. Using this information, we hypothesize that a liquid plug instilled at a slow ventilation rate into a vertically oriented lung will remain intact longer and, thus, deliver liquid deeper into the gravity-dependent regions of the lung than a liquid plug instilled at a fast ventilation rate. For faster ventilation rates, we hypothesize that the liquid plug will rupture more quickly, and, as a result, most of this liquid instilled from this situation will coat the large central airways. If true, these simple changes in ventilation rate could be easily implemented to optimize delivery of surfactant or drugs to different regions of the lung.

In summary, the many different protocols in the literature that are used to administer surfactant or other liquids into the lung have been developed through experience of trial and error. The present study and our laboratory's previous work (2) are designed to investigate the physical mechanisms that determine the resultant distribution of instilled liquid. The aim is to provide a scientific basis for developing delivery protocols and techniques that will enhance the desired targeting and distribution.

METHODS

Experimental Methods

The effect of respiratory rate on liquid transport and distribution in rat lungs was studied. A single small bolus (0.05 ml) of natural exogenous surfactant combined with a radiopaque tracer was slowly injected to plug the tracheal cannula of a rat. The lung was ventilated with 4-ml tidal volumes of gas that forced the liquid plug into the lung of the rat. The ventilation rate was 20 breaths/min in one group of rats and 60 breaths/min for the other group. By comparison, our laboratory's previous study (2) used a ventilation rate of 40 breaths/min. X-ray images of the first 8 breaths and the 20th breath were recorded in real time, enabling observation and statistical evaluation of macroscale liquid dynamics in the airways.

All protocols were reviewed and approved by the local Animal Studies Subcommittee and performed according to Institutional Animal Care and Use Committee guidelines and conformed to the *Guide for the Care and Use of Laboratory Animals* of the National Institutes of Health.

Surfactant material.

The surfactant used is a natural exogenous surfactant preparation made from bovine lung surfactant, Survanta (Ross Laboratories). Meglumine diatrizoate (0.6 g/ml; Sigma Chemical, St. Louis, MO) was added to the liquid surfactant mixture to increase X-ray absorbance of the liquid. The viscosity and surface tension of the surfactant and surfactant + meglumine diatrizoate (SMD) were measured previously at room temperature (2). The viscosity of surfactant and SMD was 45 and 10 cStokes, respectively. The surface tension of surfactant and SMD was 48 and 54 dyn/cm, respectively.

Animal preparation.

Lungs from 12 healthy Sprague-Dawley rats (347 ± 79 g) were prepared for study as follows. Each rat was anesthetized with pentobarbital sodium (40 mg/kg body wt ip). The trachea was clamped, dissected away from the surrounding tissue, and severed in a transverse plane. Tracheal diameters for these rats averaged 3.0 mm, which is at the lower end of preterm human tracheal diameters that range from 3 to 5 mm. The trachea was cannulated with a polyethylene tube (PE 240, OD = 0.242 cm and ID = 0.167 cm). The chest was opened. The lungs were removed, suspended vertically from the tracheal cannula, and placed in a 52-mm ID clear plastic cylinder. A small polyethylene tube (PE 50, OD = 0.097 cm and ID = 0.058 cm) was inserted into the tracheal cannula for instillation of SMD. The tracheal cannula was attached to a Columbus Instruments small animal ventilator (CIV-101, Columbus, OH). The lungs were inflated several times to ~14 mmHg transpulmonary pressure to remove any atelectasis resulting from the dissection procedure and then deflated to approximately functional residual capacity (4 mmHg transpulmonary pressure). Lungs were ventilated initially with 4-ml tidal volume at 20 breaths/min.

Experimental setup and procedure.

For the experiment, each lung was ventilated with a 4-ml tidal volume of gas containing 15% O_2, 6% CO_2, balance N_2 at a single predetermined ventilation rate: either 20 or 60 breaths/min. Before surfactant instillation, images of the empty ventilating lung were taken for baseline measurements. The imaging system consisted of a Fein-Focus FXE-100.50 X-ray tube with 3-μm focal spot, a North American Imaging AI-5830-HP image intensifier, and a Silicon Mountain Design 1M15 charge-coupled device camera (Silicon Mountain Design, Colorado Springs, CO) (Fig. 1). Projection images (two-dimensional) of the ventilating lung were collected at 30 frames/s.

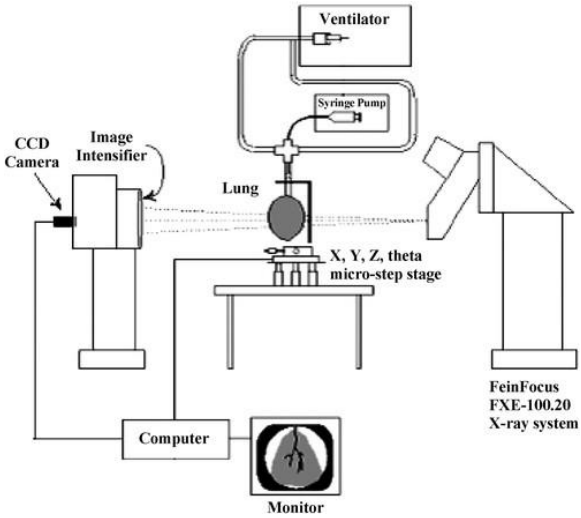

Fig. 1. Experimental setup for imaging liquid propagation in excised rat lungs. CCD, charge-coupled device.

After the empty lung was imaged, ventilation was paused at end expiration, and a 0.05-ml bolus of SMD was slowly injected into the tracheal cannula via the small polyethylene tube over 2.8 s such that the bolus formed a liquid plug in the cannula. The X-ray system was activated, and imaging of the lung began. Then, ventilation at the rate used for the baseline measurement (either 20 or 60 breaths/min) was started and continued for 20 breaths, at which point ventilation was stopped. The lung remained inflated at a transpulmonary pressure of 4 mmHg while X-ray images of the lung at this condition were collected.

Image Processing and Analysis

The transport of SMD throughout the lung is visible in the planar two-dimensional images collected by the X-ray system (Fig. 2*A*). The digitized images are 512 × 512 pixels, 8 bits/pixel, and have a numerical intensity value $I(x,y)$ ranging from 0 (black) to 255 (white) with a gray scale level between. Lung regions containing the radiopaque SMD absorbed more X-rays than empty regions and have smaller intensity values than the empty regions. For each lung image with SMD, a corresponding image of the empty lung was found with an intensity of $I_0(x,y)$ for each pixel. This image of the lung with instilled liquid is compared with an image of the empty lung (without liquid) for both image analyses.

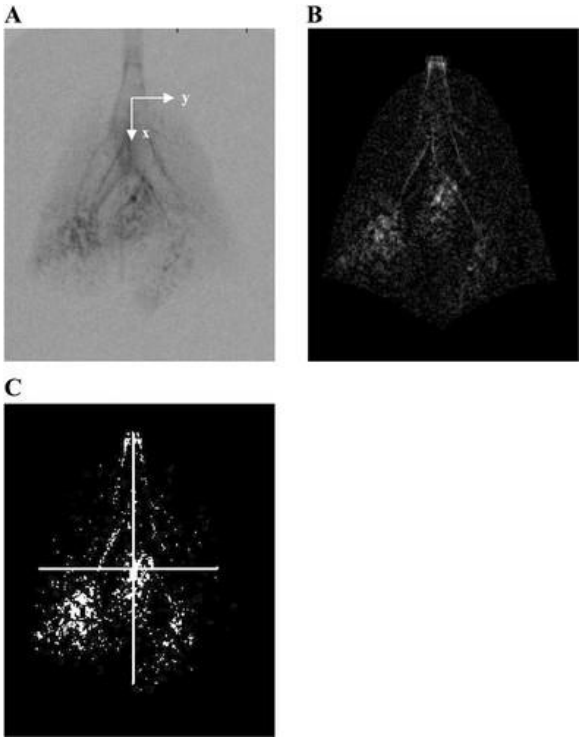

Fig. 2. *A*: X-ray image of the lung with propagating liquid with the *x* and *y* coordinate system located above the carina on an imaginary line connecting the top of the left and right lung. *B*: corresponding rat lung image without liquid has been subtracted from the image in *A*. This gray scale image, where areas with liquid are lighter, was used to calculate the statistical moments. *C*: image from *B* was thresholded to make binary and divided into quadrants.

Distribution statistics.

The first image analysis used Beer's law to determine a probability density function that described the distribution of surfactant in each lung image. The first four moments of the probability density function were calculated to further characterize this probability density function. Each image of the lung with liquid and the lung without liquid (both sampled at 30 frames/s) was loaded into Matlab (MathWorks) and converted to a double-precision matrix. Beer's law quantifies the absorbance of X-rays by the material in the image.

$$I\ (x,y) = I_0\ (x,y)e^{-mz} \quad (1)$$

I is the intensity of an image containing material, I_0 is the intensity of an image without material, *m* is the absorption coefficient of the material, and *z* is the path length of the X-ray as it travels through the material. When lung tissue is interrogated by X-rays, *Eq. 1* can be rewritten as

$$I_{\mathrm{T}}(x,y) = I_0(x,y)e^{-m_{\mathrm{T}}z_{\mathrm{T}}} \quad (2)$$

I_T is the intensity of the lung tissue, m_T is the absorption coefficient of the lung tissue, and z_T is the path length of the X-ray through the lung tissue. When X-rays pass through the lung tissue-surfactant system, *Eq. 1* can be rewritten as

$$I_{TS}(x,y) = I_0(x,y)e^{-m_{\mathrm{TS}}z_{\mathrm{TS}}} \quad (3)$$

Equation 3 describes the lung tissue and surfactant system where I_{TS} is the intensity, m_{TS} is the absorption coefficient, and z_{TS} is the path length of the X-ray for this lung tissue-surfactant system. The absorbance of X-rays

by the surfactant only ($m_S z_S$) is calculated by subtracting the lung tissue absorbance from the tissue-surfactant absorbance in a pixel-by-pixel manner. This relationship can be written in terms of intensities using *Eqs. 2* and *3*.

$$A_s(x,y) = m_S z_S(x,y) = m_{TS} z_{TS}(x,y) - m_T z_T(x,y) = log\left[\frac{I_T(x,y)}{I_{TS}(x,y)}\right] \text{ (4)}$$

The absorbance matrix, $A_S(x,y)$, was filtered by a threshold-limited process that sets pixels with a value less than a predetermined value to zero. This filtering reduced low-intensity artifacts. Additionally, $A_S(x,y)$ was cropped to eliminate extrapulmonary lung regions (Fig. 2*B*). In the resulting absorbance matrix, only the shadow of the radiopaque liquid remained visible. The origin of the (x,y) coordinates was positioned on the image above the carina on an imaginary line joining the top of the right and left lungs (Fig. 2*A*). Positive x points vertically downward along the axis of the trachea toward the carina (in the direction of gravity), and positive y points horizontally toward the right lung.

In general, a probability density function of the liquid mass was characterized so that the distribution of liquid could be quantified. For this study, a marginal probability density function was defined to calculate the distribution statistics in each direction. For example, the marginal probability density function in the vertical direction was defined as follows.

$$g(x_0) = \frac{\sum_{y=1}^{n} A_S(x_0,y)}{\sum_{x=1}^{m} \sum_{y=1}^{n} A_S(x,y)} \text{ (5)}$$

Using *Eq. 5*, we can calculate the kth moment about the x mean, $\bar{x}$.

$$M_k = \sum_{x=1}^{m} (x = \bar{x})^k \; g(x) \text{ (6)}$$

Four statistical quantities in the vertical direction were defined on the basis of the first four moments.

$$\bar{x} = M_1, \; mean\; value$$

$$\sigma_x = (M_2 - M_1^2)^{1/2}, \qquad standard\; deviation$$

$$skew_z = \frac{M_3}{\sigma_x^4}, \qquad skewness$$

$$kurt_z \frac{M_4}{\sigma_x^4} - 3, \; kurtosis \text{ (7)}$$

The skewness indicates the degree of asymmetry of the distribution around its mean. A positive (negative) skewness indicates the mean > median (mean < median), and the distribution has an asymmetrical tail extending out toward more positive (negative) direction. The kurtosis designates the relative peakedness or flatness of a distribution relative to a normal distribution. A distribution that has a positive (negative) kurtosis is more peaked (flat) than a normal distribution. By using these statistics, the shape and uniformity of the liquid distribution in the lung can be determined for both x and y directions.

Homogeneity index.

To provide a macroscopic measure of the uniformity of liquid delivery, the lungs were divided into four quadrants, and liquid deposition among these quadrants was compared to assess the homogeneity of distribution. The image of the empty lung at a given point in the breathing cycle was subtracted, pixel by pixel, from the lung image containing surfactant at the same point in the breathing cycle. A thresholding method, chosen as 10% of the gray scale, was used on the resulting image so that pixels with an absorption greater than the threshold value were given a value of one and all other pixels values were set equal to zero. All

extrapulmonary lung regions were cropped (i.e., pixel values set equal to zero). An example of a raw lung image containing surfactant and the same image processed via image subtraction and thresholding can be seen in Fig. 2, *A* and *C*. The thresholded image was divided into four main quadrants based on the center of gravity of the empty lung. To the viewer, the quadrants of the lung are labeled counterclockwise from the trachea as follows: upper left (UL), lower left (LL), lower right (LR), and upper right (UR). The thresholding method identifies pixels in the lung image where SMD is present. Within each quadrant, the number of pixels, i.e., the area reached by the liquid, is divided by the area of the quadrant. This value, the area reached (AR), is presented as a fraction of the area within the quadrant and accounts for any variation in area among the lung quadrants. The homogeneity index (HI) is defined as the smallest AR value of the four lung quadrants divided by the largest AR value of the four lung quadrants within the same image. This actually represents the minimum value of HI for distribution of liquid between any two lung quadrants. For example, if the lung quadrants are reached at a level of AR = 0.40 in LL, 0.15 in LR, 0.10 in UL, and 0.35 in UR, then HI = 0.25. If all four quadrants have the same AR value, then the distribution is considered to be 100% homogeneous (HI = 1.0) at that time in the breathing cycle, regardless of how much of the entire lung is filled. Thus the HI is a measure of the liquid that reaches a lung quadrant compared with the values in other quadrants.

RESULTS

Lung Images from Breaths 1 and 2

Figure 3 shows images of two representative lungs, one ventilated at 20 breaths/min and the other at 60 breaths/min, during the first two breaths. For each panel, the images were taken at the same lung volume and part of the ventilatory cycle. Figure 3*A* shows the two lungs after inspiration of ~16% of the first tidal volume. For the 20 breaths/min lung (Fig. 3*Aa*), the liquid has been driven into the main stem bronchi and a few smaller airways. The white arrow points to a liquid plug in upper region of the left main stem bronchi; liquid from this plug is draining via gravity down the airway wall. For the 60 breaths/min lung (Fig. 3*Ab*), the instilled plug has ruptured in the trachea and liquid has coated the walls of the trachea and upper main stem bronchi. Through the remainder of this first breath, liquid moves by gravity-driven film flow. Figure 3*B* shows the two lungs at the end of expiration of the first breath. For the 20 breaths/min lung, two plugs are present (white arrows) in the distal airways. These plugs formed during expiration as the lung decreases in volume and liquid drains into the smaller airways. On inspiration of the second breath (not shown), these plugs are driven into the terminal regions of the lung, delivering liquid to the distal lung after only two breaths. For the 60 breaths/min (Fig. 3*Bb*), liquid has moved by gravity-driven flow toward the distal end of the large airways and the base of the lung. The liquid film on the gravity-dependent side of the central airway walls appears to be thicker for the 60 breaths/min lung than the 20 breaths/min lung. The two lungs were imaged at end expiration of the second breath (Fig. 3*C*). For the 20 breaths/min lung, the liquid plugs seen in Fig. 3*Ba* have been driven into the finer structures of the gravity-dependent region of the lung. At the end of the second breath for 60 breaths/min (*Bb*), two small liquid plugs are formed in the distal main stem bronchi and indicated by two white arrows. These plugs are driven into the gravity-dependent regions of the lung on the following inspiration.

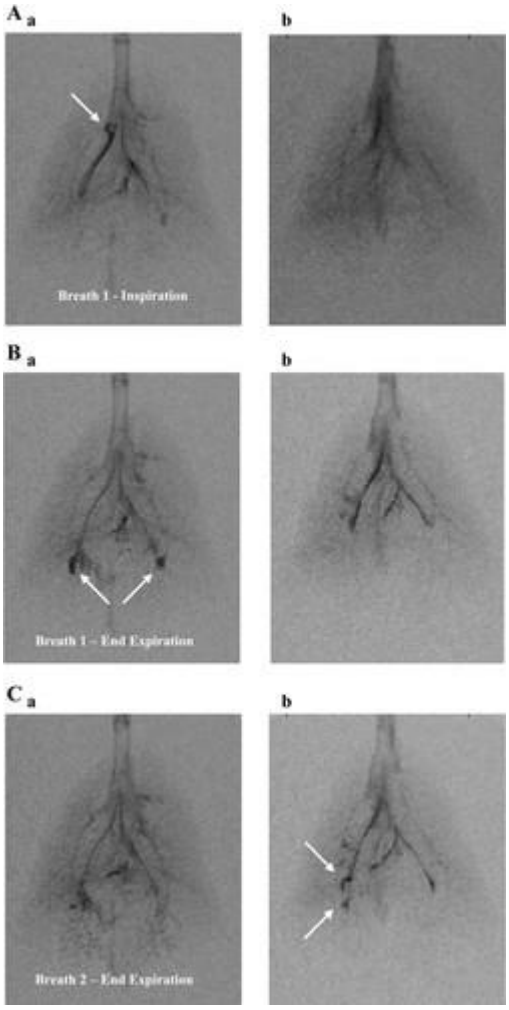

Fig. 3. Images of the rat lung ventilated at 20 breaths/min (*a*) and 60 breaths/min (*b*) during the first 2 breaths. For each panel, the images were taken at the same lung volume and part of the ventilatory cycle. White arrows point to liquid plugs. *A*: early during the 1st inspiration (~16% of tidal volume inspired), the instilled plug remains intact in the main stem bronchi of *Aa* but has already ruptured in the corresponding image of *Ab*. *B*: 2 plugs have reformed in the distal large airways of *Ba* but not in *Bb* at the end of the 1st exhalation. *C*: at the end of the 2nd exhalation, smaller plugs than seen in *Ba* have formed in *Cb* but no plugs can be seen in *Ca*.

Figure 4 is a continuation of the sequences of images in Fig. 3. The 20 breaths/min lung (*a*) and the 60 breaths/min lung (*b*) are shown at the end of expiration of *breaths 3* (*A*), *8* (*B*), and *20* (*C*). Moving from *A* to *B* to *C* for the 20 breaths/min lung, the liquid is seen progressing toward and becoming localized in the gravity-dependent region of the lung. When the 60 breaths/min lung is examined in the same manner, the liquid can be seen moving toward the gravity-dependent regions of the lung. However, a smaller portion of liquid moves to those regions and a larger amount of liquid appears to remains on the airway wall compared with the 20 breaths/min lung. A quantification of these observations is given by the distribution statistics.

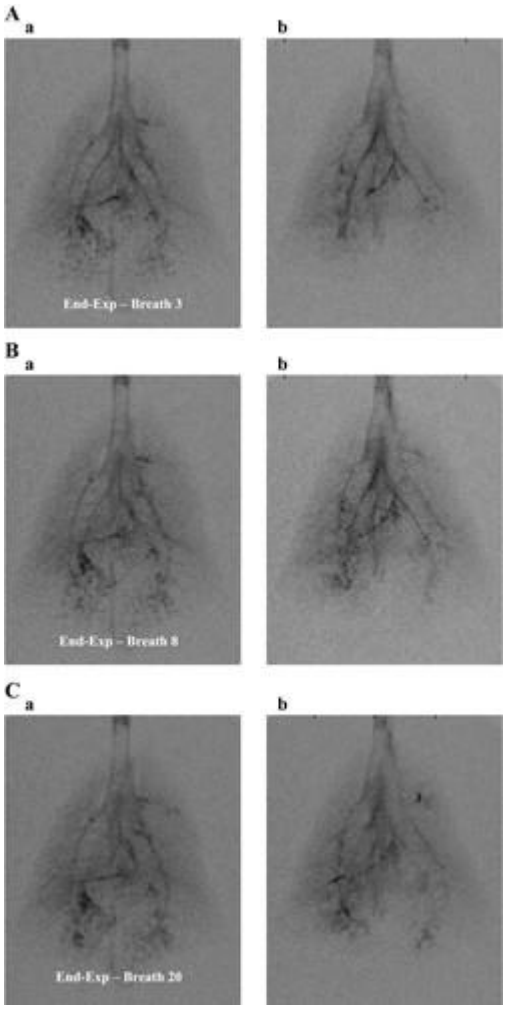

Fig. 4. Continuation of image sequence from lungs in Fig. 3 showing end expiration at 3rd (*A*), 8th (*B*), and 20th (*C*) breaths. At 20 breaths/min (*a*), the instilled liquid plug remains intact, allowing propagation of liquid to medium-sized bronchi where gravity can drain these smaller plugs toward the bottom of the lung. This shifts the liquid distribution toward the dependent lung region. At 60 breaths/min (*b*), the instilled liquid plug ruptures, causing the content to be deposited onto proximal (upper) airway walls. The influence of gravity then acts to distribute the liquid film more uniformly by the 20th breath. See Fig. 7.

Statistical Analysis

Comparison per breath.

Figure 5 shows the vertical mean (*A*), standard deviation (*B*), skewness (*C*), and kurtosis (*D*) at end expiration. The average value of each of these distribution statistics from the 20 breaths/min and 60 breaths/min group was plotted with error bars for *breaths 1–8* and *20*. Statistical differences between groups at each breath were calculated by using a two-tailed Student's *t*-test where $P < 0.05$. The mean and standard deviation were normalized by the length of the lung at end-expiratory lung volume. Figure 5*A* shows that the location of the vertical mean of the distribution increases with breath number for both groups. The mean of the 20 breaths/min group is statistically greater, i.e., further downward, than the 60 breaths/min for all breaths studied. The standard deviation (Fig. 5*B*) is statistically similar for both groups and remains fairly constant with respect to breath number. The skewness (Fig. 5*C*) for both groups decreased with breath number and was negative at the final breath, *breath 20*. This indicates that the distribution has a long tail extending from the gravity-dependent region of the lung to the trachea (see Fig. 8). The 20 breaths/min group had a statistically more negative

skewness for all breaths compared with the 60 breaths/min group. The kurtosis increases with breath number and becomes positive after *breath 3* for the 20 breaths/min group. This means the distribution in the 20 breaths/min group becomes more peaked compared with a normal distribution with increasing breath number. In contrast, the kurtosis for the 60 breaths/min group remains negative for all breaths studied. This indicates that the liquid distribution in the 60 breaths/min group is flatter than a normal distribution for all breaths (see Fig. 8). The kurtosis is statistically different between the two groups for *breaths 4* through *20*.

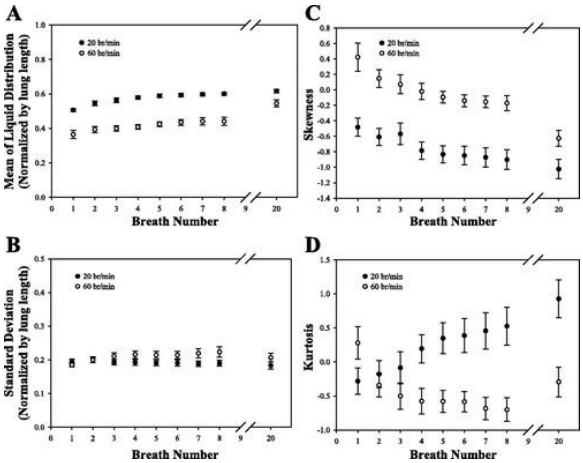

Fig. 5. Average vertical (*x*) statistical measures of liquid distribution by breath for both 20 breaths/min (•) and 60 breaths/min (○); *N* = 6 for each of these 2 groups. *A*: mean of the liquid distribution is normalized by the length of the lung and is statistically greater (i.e., toward the dependent lung) for 20 breaths/min than 60 breaths/min for *breaths 1–20*. *B*: standard deviation is normalized by the lung length and is statistically similar for the 2 liquid distributions for all breaths. *C*: skewness of the 20 breaths/min distribution is statistically less than that for the 60 breaths/min for all breaths, indicating that liquid in the 20 breaths/min distribution is more localized in the dependent lung than the 60 breaths/min. See Fig. 9. *D*: kurtosis of the 60 breaths/min group is less than the 20 breaths/min group for *breaths 4–20*, indicating that the 60 breaths/min group has a flatter vertical distribution.

In the horizontal direction, all statistical measures are statistically equivalent between groups for all breaths studied except for the kurtosis. For *breaths 1–8* and *20*, the mean of the distributions is ~0.5, the standard deviation for the distributions is ~0.15, and the skewness is ~0 for both 20 and 60 breaths/min. For 20 breaths/min, the kurtosis is zero at *breath 1* and decreases steadily to about −0.5 at *breath 20*. This means the horizontal liquid distribution for 20 breaths/min is slightly less peaked than a normal distribution. For 60 breaths/min, the kurtosis has a value of 2 at *breath 1*, has a value of 1 at *breath 2*, and decreases steadily to ~0.2 at *breath 8*. Over these first eight breaths, the horizontal kurtosis is significantly larger and positive for 60 breaths/min than 20 breaths/min, meaning the horizontal distribution for 60 breaths/min is more peaked than that for 20 breaths/min. At *breath 20*, the horizontal kurtosis is statistically similar for the two groups at about −0.5.

Comparison per time.

In addition to comparing the two groups of animals per breath, we also compared the average value of each distribution statistics between groups with respect to time. The comparisons were made at 1-s intervals starting at 0.9 s postinstillation (i.e., end expiration of the first breath for 60 breaths/min) and continuing for the first 15 s and then at the 20th second. The trends for each distribution statistic followed those described in *Comparison per breath*. Between the two groups, three distribution statistics were significantly different. The vertical mean of the distribution was statistically larger for 20 breaths/min than 60 breaths/min at all time points considered. The vertical skewness was statistically different between the two groups for the first 15 time points only. After the sixth time point, the vertical kurtosis was statistically larger for 20 breaths/min than 60 breaths/min for the

remaining time points. Over this interval, the 20 breaths/min had a positive kurtosis whereas the 60 breaths/min had a negative kurtosis. The horizontal kurtosis, although statistically different when compared per breath, was not statistically different between groups when compared with respect to time.

AR and HI

AR per breath.

Figure 6 shows the AR for each lung quadrant for the 20 breaths/min group (Fig. 6*A*) and the 60 breaths/min group (Fig. 6*B*). These AR values are plotted with error bars at end expiration for *breaths 1–8* and *20*. For both groups, the lower two quadrants AR values increase with breath number whereas the upper two quadrants AR values decrease with breath number. However, for 60 breaths/min, the upper quadrants have larger AR values than the lower quadrants over the first four breaths, and AR values for all quadrants converge toward ~0.13 at *breath 20*. For 20 breaths/min, the AR value for the LL quadrant increases rapidly after the first breath and reaches ~0.22 at *breath 20*, and the AR values of the other three quadrants converge to ~0.1 at *breath 20*. Statistical differences between groups at each breath were calculated by using a two-tailed Student's *t*-test where $P < 0.05$. The AR value of each quadrant for 20 breaths/min was compared with its corresponding quadrant for 60 breaths/min with respect to breath. A statistical difference was not found in AR values between groups for the UL and LR at any breath number studied. The AR value for the LL at 20 breaths/min was statistically larger than that value at 60 breaths/min for *breaths 1–8*. At 60 breaths/min, the AR value for the UR was statistically larger than that value at 20 breaths/min for *breaths 1–8*. When the AR value of each quadrant for 20 breaths/min is compared with its corresponding quadrant for 60 breaths/min with respect to time, the same statistical differences were found as described above.

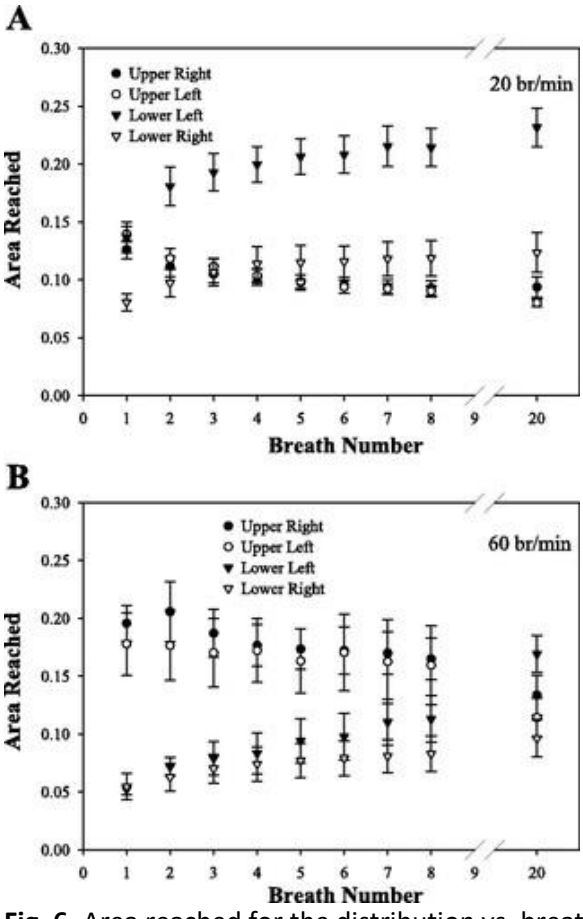

Fig. 6. Area reached for the distribution vs. breath is presented for 20 breaths/min (*A*) and 60 breaths/min (*B*) for the 4 lung regions studied. The area reached for upper right is statistically greater for the 60 breaths/min

group than the 20 breaths/min group. The area reached for lower left is statically greater for 20 breaths/min than 60 breaths/min.

HI.

The average HI for 20 breaths/min and 60 breaths/min at end expiration was plotted with error bars for *breaths 1–8* and *20* (Fig. 7). For 20 breaths/min, HI has a value of ~0.5 at *breath 1* and decreases to ~0.37 at *breath 20*. For 60 breaths/min, the value of HI is ~0.22 at *breath 1* and increases to ~0.45 at *breath 20*. The two trends of HI vs. breath appear to intersect at *breath 7*. The value of HI for 20 breaths/min is statistically greater than 60 breaths/min for *breaths 1–3* and statistically less than 60 breaths/min for *breath 20*. With respect to time, the value of HI for 20 breaths/min is statistically greater than 60 breaths/min for the first 4 s and is statistically less than 60 breaths/min at the 20th second.

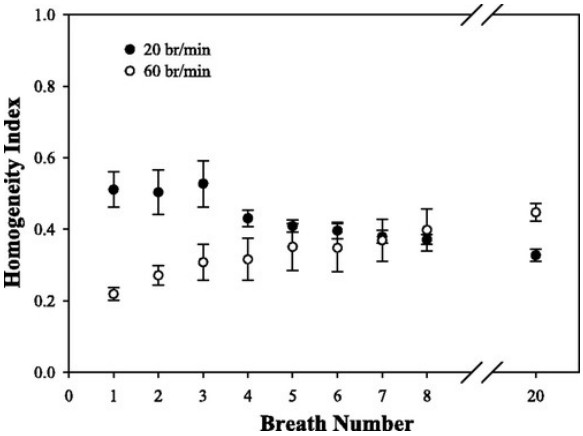

Fig. 7. Homogeneity indexes (HI) for 20 breaths/min (•) and 60 breaths/min (○) are presented vs. breath number. For the first 3 breaths, the 20 breaths/min group has a statistically greater HI than 60 breaths/min group. By the 20th breath, this relationship has reversed. The 60 breaths/min group has a greater HI than 20 breaths/min group.

DISCUSSION

To appreciate more fully the results of the vertical statistics, we have plotted the vertical distribution of a representative animal from the 20 breaths/min group and 60 breaths/min group in Fig. 8. On the ordinate, the vertical lung position has been normalized by the length of the lung where zero indicates the top (i.e., the location of the coordinate system) and one indicates the bottom of the lung. The marginal probability density lies on the abscissa and is given by *Eq. 5*. The mean of each distribution is indicated by a solid line and the median (i.e., 50th percentile) of each distribution is indicated by a dashed line. Both of these distributions correspond to the given lung at end expiration of *breath 6* and are representative of the average statistical values presented in Fig. 5. From Fig. 8, the vertical distribution of 60 breaths/min is more uniform than that of 20 breaths/min. First, the 60 breaths/min distribution is relatively flat and the 20 breaths/min distribution is relatively peaked compared with a normal distribution. This feature of the distribution is summarized in the kurtosis statistic, in which a negative kurtosis (60 breaths/min) indicates a flatter distribution and a positive kurtosis (20 breaths/min) indicates a peaked distribution. Second, the 20 breaths/min distribution is more skewed, toward the trachea in this case, than the 60 breaths/min. The skewness of the distribution quantifies the difference between the mean and the median of the distribution. A negative skewness indicates the median of the distribution is shifted to the right (i.e., into the dependent lung) of the mean. Thus a majority of the distribution's mass resides further downward in relation to the mean. For Fig. 8, the skewness is negative for both distributions but more negative for the 20 breaths/min distribution than 60 breaths/min. The difference

between the mean and median is larger for 20 breaths/min than 60 breaths/min and, thus, a larger majority of the mass of the 20 breaths/min distribution resides to the right of the mean.

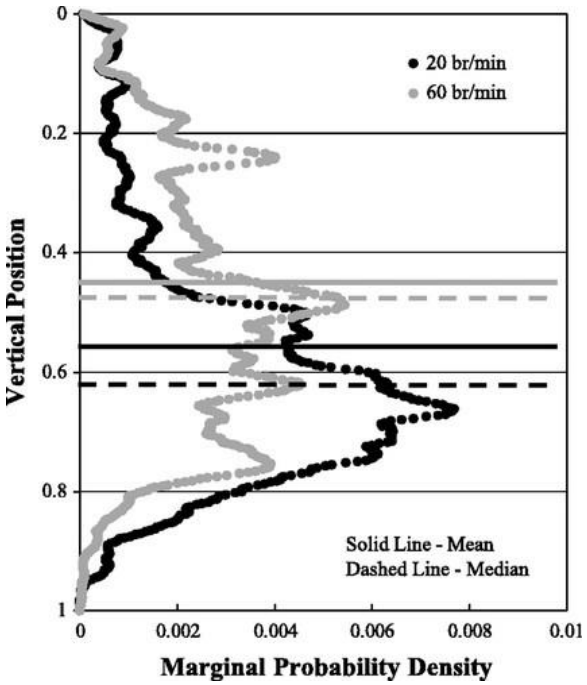

Fig. 8. Example of vertical liquid distributions in 2 conditions as given by the marginal probability density function, $g(x_0)$; see *Eq. 5*. One distribution is at 20 breaths/min (black circles) and the other is at 60 breaths/min (gray circles). The data have been smoothed with an 11-point moving average. These raw results reflect the average statistical measures presented in Fig. 5 for *breath 6*.

Using the picture of the vertical distribution provided by Fig. 8, we examined the vertical distribution results summarized in Fig. 5. For the 20 breaths/min group, we notice that the mean of the distribution increases, the skewness decreases to become more negative, and the kurtosis increases to become more positive with breath number. These results show that the 20 breaths/min delivers liquid vertically deeper into the lung with each breath (mean), and most of the liquid becomes localized in sites that are deeper in the lung than the mean of the distribution (skewness and kurtosis) with each breath. Relative to the 20 breaths/min results, the 60 breaths/min mean is less, the skewness is less negative, and the kurtosis is negative. Thus 60 breaths/min has a more uniform vertical distribution relative to 20 breaths/min at each breath.

In Fig. 6, notice that in the first breath for 20 breaths/min and the first four breaths for 60 breaths/min, the upper quadrants have larger AR values than the lower quadrants for both frequencies. This fact is because the liquid must travel through the upper lung quadrants before reaching the lower quadrants. With increasing breath number for 60 breaths/min, the upper quadrant AR values decrease as liquid drains from the upper lung into regions of the lower lung without liquid causing the lower region AR values to increase. Thus, with increasing breath number, the AR value in all quadrants converge to similar values. This increase in homogeneity between regions is summarized by HI in Fig. 7. HI increases with increasing breath number for 60 breaths/min. In contrast, HI decreases for 20 breaths/min because with increasing breaths liquid becomes more localized in the gravity-dependent part of the lung. For this homogeneity analysis, the liquid is localized to the LL quadrant. This result is similar to the statistical moment analysis finding. The liquid distributions after *breath 3* appear to be the result of plug propagation and gravity mechanisms on the initial liquid instillation.

In our study, the liquid properties are the same in both groups of rats. Thus the thickness of the trailing film on the airway walls is directly related to instillation speed or respiratory rate, which determines *U* in the capillary number. As a corollary, the time to plug rupture is inversely related to instillation speed. With a rapid instillation (60 breaths/min), a thicker liquid film is deposited on the airway wall and the instilled plug ruptures relatively quickly after instillation. In contrast, the slower instillation of liquid (20 breaths/min) promotes a thinner trailing film of liquid on the airway wall and maintains an intact plug for a longer period of time (see Fig. 3, *A* and *B*). As a result, a larger portion of the instilled liquid is delivered to the gravity-dependent portions of the lung within a few breaths for 20 breaths/min, but for 60 breaths/min most of the instilled liquid is initially deposited on the walls of the larger, central airways.

The presence of liquid plugs in the airways appeared to be a crucial feature to determining liquid delivery. To quantify this effect, we estimated the volume of each plug in the larger airways during the first 3 s of liquid instillation for both groups. This estimate was made by assuming a cylindrical plug shape that was evenly bisected by the plane of the image giving its length and diameter. The volumes of these plugs were summed for each image and normalized by the volume of the initial instilled plug. This normalized, total plug volume for each image was plotted vs. time in Fig. 9 for a representative 20 breaths/min lung (Fig. 9*B*) and 60 breaths/min lung (Fig. 9*A*). To each panel we added a tracing of normalized lung volume vs. time where 0 is end-expiratory lung volume and 1 is end-inspiratory lung volume. The right axis provides a scale for this curve. For 20 breaths/min, a plug is seen early in the inspiratory phase, which corresponds to the plug seen in Fig. 3*Aa*. We assume that this plug was present in the trachea before we detected it in the main stem bronchi, but we could not clearly define the plug size because its speed caused it to be blurred in those images. At the end of inspiration, plugs begin to reform in the distal airways of the main stem bronchi and grow in size as liquid drains down the airway wall. An image of these plugs can be seen in Fig. 3*Ba*. For the 60 breaths/min lung, plugs are detected in the distal airways at the end of expiration of the second breath (see Fig. 3*Cb*) and again at the end of the third expiration. The normalized total plug volume for the 60 breaths/min plugs is, on average, smaller than the total seen in the 20 breaths/min lung. In summary, for the 20 breaths/min group, in which liquid was preferentially delivered to the gravity-dependent regions of the lung, liquid plugs are larger and maintained for longer periods of time for than the 60 breaths/min group, in which the liquid initially coated the more central airways and provided a vertically uniform liquid distribution after 20 breaths.

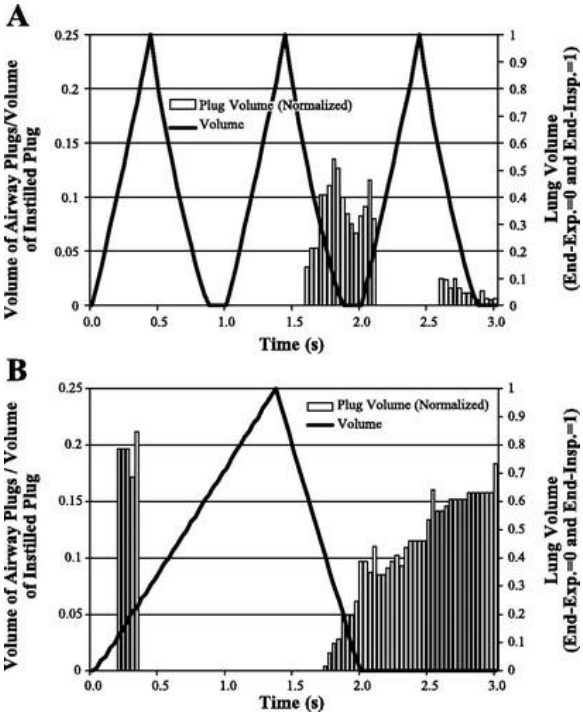

Fig. 9. During the first 3 s of liquid instillation, the volume of all liquid plugs in large airways was calculated for each image and normalized by the volume of the initial instilled plug. This normalized plug volume is plotted on the left axis and a normalized lung volume (0 = end-expiratory lung volume; 1 = end-inspiratory lung volume) is on the right axis, with time in seconds across the bottom. Over this 3-s period, more of the instilled liquid is found as airway plugs over a longer period of time for the 20 breaths/min lung (*B*) than the 60 breaths/min lung (*A*).

In addition to the plug propagation mechanisms, gravity acts on the liquid to transport it down the airway wall toward the dependent lung. For the slow ventilation rate (20 breaths/min), long dead times between end expiration and the start of the subsequent inspiration are present (Fig. 9*B*). Over this time, gravity acts on the liquid coating the airway walls, causing it to drain into the smaller, gravity-dependent airways where plugs can reform. This mechanism is clearly promoting plug formation from the end of expiration (time ≈ 2 s) until the start of inspiration (time = 3 s) as seen by the increase of airway plug volume in Fig. 9*B*. Thus gravity assists in liquid delivery to the dependent lung for 20 breaths/min. For the faster ventilation rate (60 breaths/min), gravity appears to smooth out the vertical distribution of liquid. Immediately after liquid instillation, the liquid plug ruptures, resulting in a thick liquid layer on the walls of the trachea and main stem bronchi. Over the subsequent breaths, this liquid layer drains down the airway wall via the force of gravity, resulting in a more uniform vertical distribution of liquid.

Conclusions

We instilled small liquid plugs (0.05 ml) of surfactant into vertically suspended excised rat lungs at two ventilation rates, 20 and 60 breaths/min, over 20 breaths. The respiratory rates reported in our study would be used during the instillation phase of surfactant delivery in an intubated patient such as a preterm newborn whose ventilation rate is determined by the use of an Ambu bag or ventilator. This phase may last only a few minutes to assist the transport of liquid to its targeted location. These locations may be central airways, lung lobes, or specific terminal regions depending on the therapy: surfactant replacement, drug delivery, or genetic material. After this initial targeted instillation is achieved, normal ventilation using an appropriate ventilation rate could be used.

At 20 breaths/min, the liquid was quickly driven into the gravity-dependent region of the lung. At 60 breaths/min, the liquid was first deposited on the airway walls and then transported toward the gravity-dependent region of the lung over the following breaths. After the 20 breaths, the liquid in the 20 breaths/min group was localized in the gravity-dependent region of the lung whereas the liquid in the 60 breaths/min group was vertically distributed in a more uniform manner throughout the lung. The cause of the liquid propagation and final liquid distribution results from the interplay of liquid plug dynamics and gravitational effects. At fast ventilation rates (60 breaths/min), an instilled liquid plug ruptures during the first inspiration, liquid coats the large central airways, and liquid drains down the airways over the following breaths via the force of gravity. At slow ventilation rates (20 breaths/min), the instilled liquid plug remains intact over most of the first inspiration, liquid plugs form via gravitational drainage after the first expiration, and the liquid is driven into the dependent lung on the second inspiration.

This study provides insight into the physical mechanisms for liquid delivery into the lung. It focuses on the early, transient behavior that dictates the resulting distribution, which may be weighted distally for slower ventilation rates or more proximally for faster rates. This information can be clinically important when using liquid as a vehicle for drug or gene delivery. Understanding the transient effects of liquid delivery will enable increased accuracy for targeted delivery of liquid carrying drugs and genetic material to central airways, lung lobes, or spatially oriented terminal regions. Our study shows that the targeting is linked to the ventilation rate. Genes, drugs, or other material can be loaded into an instilled plug for accurate delivery to a preferred pulmonary site. This knowledge allows for finer control over the dose of a material to a particular lung region and more efficient utilization of the delivered material.

For delivery of surfactants, for example, if the liquid is instilled into the terminal regions of a lobe by using a slow ventilation rate, it may be difficult to redistribute that liquid to other lobes by rotating of the patient, as is currently done in surfactant replacement therapy, to achieve a surfactant distribution that is homogeneous throughout the lung. However, if the liquid is instilled at a fast ventilation rate, the majority of the liquid should coat the airway walls and then could be directed into different lobes of the lung by rotating the patient.

GRANTS

This work was supported, in part, by National Heart, Lung, and Blood Institute Grant HL-41126 and National Aeronautics and Space Administration Grant NAG3-2740.

FOOTNOTES

- The costs of publication of this article were defrayed in part by the payment of page charges. The article must therefore be hereby marked "*advertisement*" in accordance with 18 U.S.C. Section 1734 solely to indicate this fact.

We are grateful to Ross Laboratories for donation of the surfactant.

REFERENCES

1 Bretherton FP**.** The motion of long bubbles in tubes. ***J Fluid Mech*** *10*: 166–188, 1961.

2 Cassidy KJ**, Bull JL, Glucksberg MR, Dawson CA, Haworth ST, Hirschl RB, Gavriely N, and Grotberg JB.** A rat lung model of instilled liquid transport in the pulmonary airways. ***J Appl Physiol*** *90*: 1955–1967, 2001.

3 Cassidy KJ**, Gavriely N, and Grotberg JB.** Liquid plug flow in straight and bifurcating tubes. ***J Biomech Eng*** *123*: 580–589, 2001.

4 Chung EH**, Ko SY, Kim IY, Chang YS, and Park WS.** Changes in dead space/tidal volume ratio and pulmonary mechanics after surfactant replacement therapy in respiratory distress syndrome of the newborn infants. ***J Korean Med Sci*** *16*: 51–56, 2001.

5 Corbet A**, Bucciarelli R, Goldman S, Mammel M, Wold D, and Long W.** Decreased mortality rate among small premature infants treated at birth with a single dose of synthetic surfactant: a multicenter controlled trial. ***J Pediatr*** *118*: 277–284, 1991.

6 Davis JM**, Russ GA, Metlay L, Dickerson B, and Greenspan BS.** Short-term distribution kinetics of intratracheally administered exogenous lung surfactant. ***Pediatr Res*** *31*: 445–450, 1992.

7 Dickson EW**, Heard SO, Tarara TE, Weers JG, Brueggemann AB, and Doern GV.** Liquid ventilation with perflubron in the treatment of rats with pneumococcal pneumonia. ***Crit Care Med*** *30*: 393–395, 2002.

8 Espinosa FF **and Kamm RD.** Bolus dispersal through the lungs in surfactant replacement therapy. ***J Appl Physiol*** *86*: 391–410, 1999.

9 Espinosa FF **and Kamm RD.** Meniscus formation during tracheal instillation of surfactant. ***J Appl Physiol*** *85*: 266–272, 1998

10 Feldbaum DM**, Wormuth D, Nieman GF, Paskanik M, Clark WR, and Hakim TS.** Exosurf treatment following wood smoke inhalation. ***Burns*** *19*: 396–400, 1993.

11 Fuhrman BP**, Paczan PR, and DeFrancisis M.** Perfluorocarbon-associated gas exchange. ***Crit Care Med*** *19*: 712–722, 1991.

12 Gilliard N**, Richman PM, Merritt TA, and Spragg RG.** Effect of volume and dose on the pulmonary distribution of exogenous surfactant administered to normal rabbits or to rabbits with oleic acid lung injury. ***Am Rev Respir Dis*** *141*: 743–747, 1990.

13 Goldsmith LS**, Greenspan JS, Rubenstein SD, Wolfson MR, and Shaffer TH.** Immediate improvement in lung volume after exogenous surfactant: alveolar recruitment versus increased distention. ***J Pediatr*** *119*: 424–428, 1991.

14 Halpern D **and Gaver DP.** Boundary-element analysis of the time-dependent motion of a semi-infinite bubble in a channel. ***J Comp Physiol*** *115*: 366–375, 1994.

15 Halpern D**, Jensen OE, and Grotberg JB.** A theoretical study of surfactant and liquid delivery into the lung. ***J Appl Physiol*** *85*: 333–352, 1998.

16 Heldt GP**, Merritt TA, Golembeski D, Gilliard N, Bloor C, and Spragg R.** Distribution of surfactant, lung compliance, and aeration of preterm rabbit lungs after surfactant therapy and conventional and high-frequency oscillatory ventilation. ***Pediatr Res*** *31*: 270–275, 1992.

17 Howell PD**, Waters SL, and Grotberg JB.** The propagation of a liquid bolus along a liquid-lined flexible tube. ***J Fluid Mech*** *406*: 309–335, 2000.

18 Jobe AH**.** Pulmonary surfactant therapy. ***N Engl J Med*** *328*: 861–868, 1993.

19 Kendig JW**, Notter RH, Cox C, Reubens LJ, Davis JM, Maniscalco WM, Sinkin RA, Bartoletti A, Dweck HS, Horgan MJ, Risemberg H, Phelps DL, and Shapiro DL.** A comparison of surfactant as immediate prophylaxis and as rescue therapy in newborns of less than 30 weeks gestation. ***N Engl J Med*** *324*: 865–871, 1991.

20 Krause MF**, Jakel C, Haberstroh J, Schulte-Monting J, Leititis JU, and Orlowska-Volk M.** Alveolar recruitment promotes homogeneous surfactant distribution in a piglet model of lung injury. ***Pediatr Res*** *50*: 34–43, 2001.

21 Leach CL**, Fuhrman BP, Morin FC, and Rath MG.** Perfluorocarbon-associated gas exchange (partial liquid ventilation) in respiratory distress syndrome: a prospective, randomized, controlled study. ***Crit Care Med*** *21*: 1270–1278, 1993.

22 Lewis J**, McCaig L, Hafner D, Spragg R, Veldhuizen R, and Kerr C.** Dosing and delivery of a recombinant surfactant in lung-injured adult sheep. ***Am J Respir Crit Care Med*** *159*: 741–747, 1999.

23 Lewis JF **and Jobe AH.** Surfactant and the adult respiratory distress syndrome. ***Am Rev Respir Dis*** *147*: 218–233, 1993.

24 Long W**, Thompson T, Sundell H, Schumacher R, Volberg F, and Guthrie R.** Effects of two rescue doses of a synthetic surfactant on mortality rate and survival without bronchopulmonary dysplasia in 700- to 1350-gram infants with respiratory distress syndrome. The American Exosurf Neonatal Study Group I. ***J Pediatr*** *118*: 595–605, 1991.

25 Matalon S**, Holm BA, and Notter RH.** Mitigation of pulmonary hyperoxic injury by administration of exogenous surfactant. ***J Appl Physiol*** *62*: 756–761, 1987.

26 Novick RJ**, Veldhuizen RA, Possmayer F, Lee J, Sandler D, and Lewis JF.** Exogenous surfactant therapy in thirty-eight hour lung graft preservation for transplantation. ***J Thorac Cardiovasc Surg*** *108*: 259–268, 1994.

27 Ogawa Y **and Shimizu H.** Current strategy for management of meconium aspiration syndrome. ***Acta Paediatr Taiwan*** *41*: 241–245, 2000.
28 Park CW **and Homsy GM.** Two-phase displacement in hele shaw cells: theory. ***J Fluid Mech*** *139*, 291–308, 1984.
29 Pataki G**, Czopf L, Holm BA, and Matalon S.** Quantitation of the alveolar distribution of surfactant mixtures in normal and injured lungs. ***Am J Respir Cell Mol Biol*** *15*: 451–459, 1996.
30 Rider ED**, Jobe AH, Ikegami M, and Sun B.** Different ventilation strategies alter surfactant responses in preterm rabbits. ***J Appl Physiol*** *73*: 2089–2096, 1992.
31 Segerer H**, van Gelder W, Angenent FW, van Woerkens LJ, Curstedt T, Obladen M, and Lachmann B.** Pulmonary distribution and efficacy of exogenous surfactant in lung-lavaged rabbits are influenced by the instillation technique. ***Pediatr Res*** *34*: 490–494, 1993.
32 Smith DJ**, Gambone LM, Tarara T, Meays DR, Dellamary LA, Woods CM, and Weers J.** Liquid dose pulmonary instillation of gentamicin PulmoSpheres formulations: tissue distribution and pharmacokinetics in rabbits. ***Pharm Res*** *18*: 1556–1561, 2001.
33 Spragg RG**, Lewis JF, Wurst W, Hafner D, Baughman RP, Wewers MD, and Marsh JJ.** Treatment of acute respiratory distress syndrome with recombinant surfactant protein C surfactant. ***Am J Respir Crit Care Med*** *167*: 1562–1566, 2003.
34 Spragg RG**, Smith RM, Harris K, Lewis J, Hafner D, and Germann P.** Effect of recombinant SP-C surfactant in a porcine lavage model of acute lung injury. ***J Appl Physiol*** *88*: 674–681, 2000.
35 Taylor GI**.** Deposition of a viscous fluid on the wall of a tube. ***J Fluid Mech*** *10*: 161–165, 1961.
36 Tutuncu AS**, Akpir K, Mulder P, Erdmann W, and Lachmann B.** Intratracheal perfluorocarbon administration as an aid in the ventilatory management of respiratory distress syndrome. ***Anesthesiology*** *79*: 1083–1093, 1993.
37 Ueda T**, Ikegami M, Rider ED, and Jobe AH.** Distribution of surfactant and ventilation in surfactant-treated preterm lambs. ***J Appl Physiol*** *76*: 45–55, 1994.
38 Vazquez de Anda GF**, Lachmann RA, Gommers D, Verbrugge SJ, Haitsma J, and Lachmann B.** Treatment of ventilation-induced lung injury with exogenous surfactant. ***Intensive Care Med*** *27*: 559–565, 2001.
39 Waters SL **and Grotberg JB.** The propagation of a surfactant laden liquid plug in a capillary tube. ***Phys Fluids*** *14*: 471–480, 2002.
40 Weiss DJ**, Strandjord TP, Jackson JC, Clark JG, and Liggitt D.** Perfluorochemical liquid-enhanced adenoviral vector distribution and expression in lungs of spontaneously breathing rodents. ***Exp Lung Res*** *25*: 317–333, 1999.
41 Weiss DJ**, Strandjord TP, Liggitt D, and Clark JG.** Perflubron enhances adenovirus-mediated gene expression in lungs of transgenic mice with chronic alveolar filling. ***Hum Gene Ther*** *10*: 2287–2293, 1999.
42 Wiswell TE**, Peabody SS, Davis JM, Slayter MV, Bent RC, and Merritt TA.** Surfactant therapy and high-frequency jet ventilation in the management of a piglet model of the meconium aspiration syndrome. ***Pediatr Res*** *36*: 494–500, 1994.
43 Wolfson MR**, Greenspan JS, Deoras KS, Rubenstein SD, and Shaffer TH.** Comparison of gas and liquid ventilation: clinical, physiological, and histological correlates. ***J Appl Physiol*** *72*: 1024–1031, 1992.